

Long-base seismic interferometry reveals a hidden slow-slip event near the Anza seismic gap

Yixiao Sheng¹, Aurélien Mordret¹, Korbinian Sager^{2,3}, Florent Brenguier¹, Pierre Boué¹, Baptiste Rousset¹, Frank Vernon⁴, Yehuda Ben-Zion⁵

1. University Grenoble Alpes, 2. Brown University, 3. Ludwig Maximilian University of Munich, 4. University of California, San Diego, 5. University of Southern California

Introduction

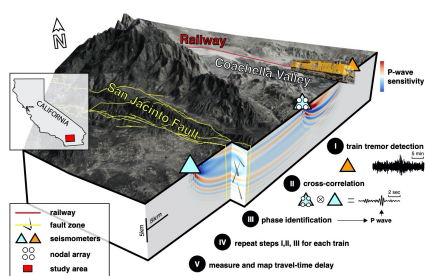
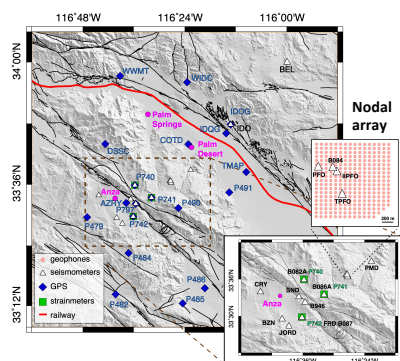


Fig. 1. Schematic illustration of the location and layout of the study site and the data processing.

We use seismic tremors generated by large freight trains as repeatable sources to construct body wave correlation functions for monitoring seismic velocity changes associated with fault movements. We focus on the San Jacinto Fault Zone in the Anza area, CA. This area is densely equipped with geophysical instruments, with large freight trains regularly running through the nearby Coachella Valley.

Train detection



We use the Piñon Flat Observatory as the anchor site, where there are permanent seismic stations, accompanied by a temporary nodal array for tracking moving trains and for examining the feasibility of retrieving body waves in correlation functions.

Fig. 2. Map of the study area with geophysical instrument networks

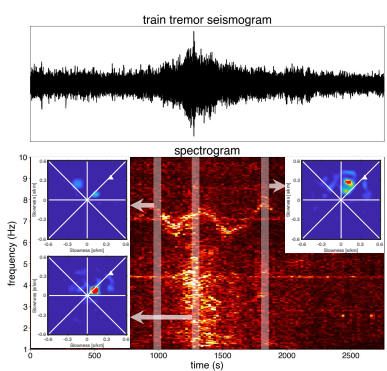


Fig. 3. Train tremor and beamforming using the temporary nodal array

The beamforming results suggest train-generated P-wave energy peaks in the study area when trains are passing by station CI.IDO. We use this seismic station as a marker to time trains and construct a train catalog.

Reference

J. Lin, R. S. Stein, Stress triggering in thrust and subduction earthquakes and stress interaction between the southern San Andreas and nearby thrust and strike-slip faults. *J. Geophys. Res. Solid Earth* 109, B02303 (2004).
 J. Jiang, Y. Fialko, Reconciling seismicity and geodetic locking depths on the Anza section of the San Jacinto Fault. *Geophys. Res. Lett.* 43(20), 10-663 (2016).
 K. Sager et al., <https://eartharxiv.org/repository/view/2469> (2021).
 S. Mao, A. Mordret, M. Campillo, H. Fang, R. D. van der Hilst, On the measurement of seismic travel-time changes in the time-frequency domain with wavelet cross-spectrum analysis. *Geophys. J. Int.* 221(1), 550-568 (2020).
 Z. E. Ross, D. T. Trugman, E. Hauksson, P. M. Shearer, Searching for hidden earthquakes in southern California. *Science* 364(6442), 767-771 (2019).

Results

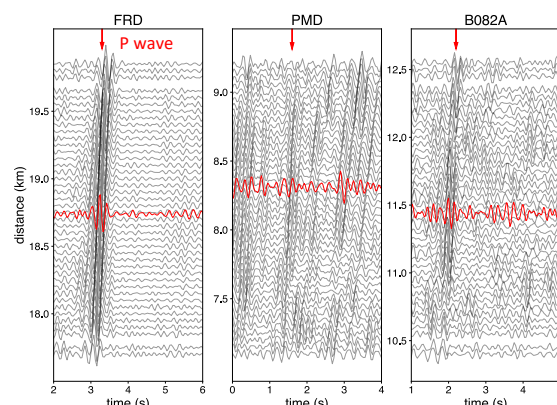


Fig. 5. Examples of station-station correlation functions (red) from station II.PFO at the Piñon Flat Observatory to stations AZ.FRD, CI.PMD, and PB.B082A, accompanied by the array-station correlation functions (black).

The correlation functions constructed from train-generated seismic signals are suitable for long-term seismic monitoring.

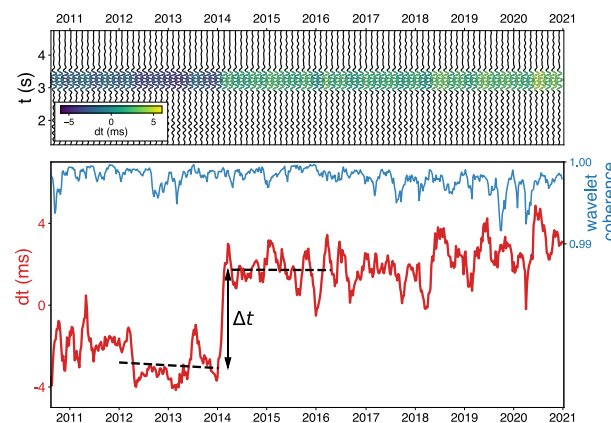


Fig. 6. Long-term travel-time perturbations for station pair II.PFO-AZ.FRD.

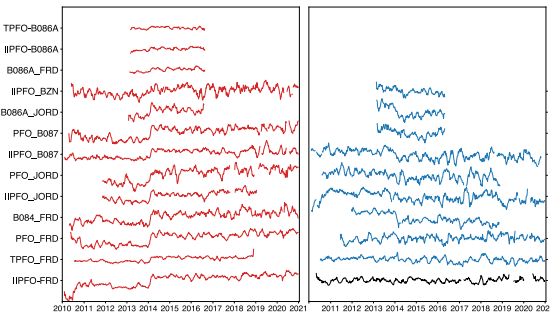


Fig. 7. Long-term travel-time perturbations for all station pairs.

We measure the travel-time perturbation with respect to the long-term average using the wavelet methods (Mao et al., 2020). In early 2014, some station pairs exhibit positive time shift (velocity drop) while others show negative time shift (velocity increase).

Interpretation

We hypothesized that the velocity change is produced by a slow-slip event, which alters volumetric strain and leads to the opening and closure of cracks or voids. We test this hypothesis using numerical simulations. The Coulomb software (Lin and Stein, 2004) is used to simulate volumetric strain, which is converted to seismic velocity change (dV/V) through velocity-stress sensitivity. The modeled dV/V is then mapped to travel-time differences using full-waveform simulations of correlation functions with and without velocity perturbations (Sager et al., 2021).

Fig. 8. Examples of modeled correlation functions and P-wave sensitivity kernels for station pairs II.PFO-AZ.FRD (A) and II.PFO-AZ.CRY (B). The simulated correlation functions match the observations very well

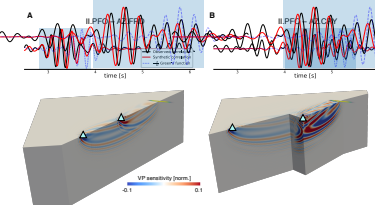


Table 1. The preferred slow-slip dislocation model

Starting latitude	Starting longitude	Ending latitude	Ending longitude	Depth (km)	Right lateral slip (cm)	Dip (°)	Rake (°)
33.5113	-116.5470	33.5330	-116.5814	6-8	20	90	180

We find a preferred dislocation model that explains the observations reasonably well. The parameters are given in Table 1.

Fig. 9. Measurements and simulations associated with the 2014 velocity perturbation. The background color in the top panel shows the volumetric strain at 1km depth from the preferred dislocation model. Its surface projection is indicated by the thick black line

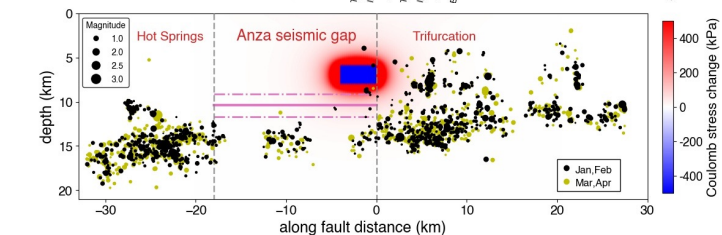
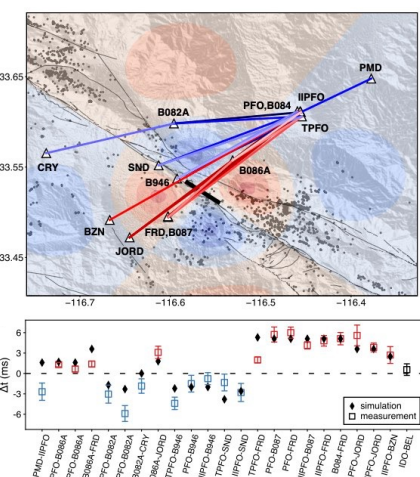


Fig. 10. Along-fault view of the inverted slow-slip patch, the associated Coulomb stress change and the seismicity in the vicinity of the fault. Earthquakes are from the QTM catalog (Ross et al., 2019). The magenta color marks the geodetic locking depth (Lindsey et al., 2014).

The inverted slow-slip event is slightly shallower than the geodetic locking depth (Lindsey et al., 2014) and locates at the southern end of the seismic gap, at the transition to the zone with high seismic activity. It suggests a transition zone with heterogeneous mechanical properties, which is consistent with earthquake cycle simulations (Jiang and Fialko, 2016).

Acknowledgement

All the seismic waveform data used can be accessed through IRIS. Both the borehole strainmeter data and GPS data are obtained from UNAVCO (<https://www.unavco.org>). This study was funded by the European Research Council (ERC) under Grant Agreement Number 817803 (FAULTSCAN) and 742335 (F-IMAGE).